PHYSICAL REVIEW A VOLUME 27, NUMBER 6 JUNE 1983

Photoelectron measurements of the mercury $4f$, $5p$, and $5d$ subshells

P. H. Kobrin, P. A. Heimann, H. G. Kerkhoff,* D. W. Lindle, C. M. Truesdale, T. A. Ferrett, U. Becker,* and D. A. Shirley

Materials and Molecular Research Division, Lawrence Berkeley Laboratory, Berkeley, California 94720 and Department of Chemistry, University of California, Berkeley, California 94720

(Received 22 November 1982)

Photoelectron spectra of atomic mercury have been taken using photon energies between 50 and 270 eV. The relative cross sections, subshell branching ratios, and angular distribution asymmetry parameters of the $4f$, $5p$, and $5d$ subshells are reported. In addition, the $4f$ asymmetry parameter was measured up to 600 eV. These quantities show dramatic effects accompanying Cooper minima in the $5d$ and $5p$ subshells and a large centrifugal barrier in the $4f \rightarrow \epsilon g$ channel. Comparisons are made with relativistic random-phase approximation and Dirac-Slater calculations. Intershell correlations appear responsible for features in the measured $4f$ asymmetry parameter at the $4d$ threshold and in the calculated $5d$ branching ratio at the $5p$ threshold.

I. INTRODUCTION

Mercury is the heaviest stable element with closed electronic subshells and an appreciable vapor pressure at low temperatures. Relativistic effects in photoionization are thus readily studied in mercury. An absorption spectrum has been reported over a wide energy range,[1] but photoemission studies have been limited to photon energies below 50 eV,[2] and to the discrete energies 132.3 eV (Ref. 3) and 1486.6 eV (Ref. 4). In this paper, we report the first photoemission studies of atomic mercury throughout the photon energy range 50–270 eV, with some additional data, based on second-order light, up to $h\nu = 600$ eV. The $4f$, $5p$, and $5d$ subshells were studied.

Several theoretical approaches, which treat exchange, correlation, and relativistic effects in varying degrees of approximation, have been developed and applied to mercury. The $4f$ partial cross section and photoelectron angular distribution have been calculated by both Shyu and Manson[5] and by Keller and Combet Farnoux[6] with both the Hartree-Slater (HS) and Hartree-Fock (HF) models. Keller and Combet Farnoux have also calculated the $5d$ and $5p$ partial cross sections. These studies highlight the influence of intrachannel interactions that are included in HF but not in HS. Walker and Waber[7] have done Dirac-Slater (DS) calculations on the $5d$ subshell. With this relativistic theory, they are able to predict the branching ratio and the spin-orbit resolved angular distributions. More recent DS calculations have been performed by Tambe and Manson[8] and by Keller and Combet Farnoux.[9] Tambe and Manson[8] have done calculations on the $4f$, $5p$, and $5d$ subshells. Keller and Combet Farnoux have done calculations on the $4f$, $5d$, and $4d$ subshells. Radojević and Johnson[10] have used the relativistic random-phase approximation (RRPA) to model the photoionization of mercury over the energy range covered by our experiment. Their method includes both relativistic effects and electron correlations (intershell as well as intrashell). They have coupled all 17 relativistic outgoing channels originating from the $4f$, $5p$, and $5d$ subshells and have calculated cross sections, branching ratios, and photoelectron angular distributions for each subshell.

Keller and Combet Farnoux[6] have pointed out that the choice of threshold energies in *ab initio* calculations affects not only the positions of features but also the shapes of the curves. In their HS and HF calculations, they used HS ionization thresholds in order to be self-consistent. On the other hand, Radojević and Johnson employed experimental binding energies in an attempt to account for some of the many-body effects not included in RRPA calculations. Tambe and Manson have used DS values. These various models differ greatly. For the $4f$ subshell, the DS binding energy lies 30 eV from the HS value, and neither is within 10 eV of experiment. The effects of changing thresholds on the shapes of the curves have not yet been fully explored.

The experiment is described in Sec. II. Results are presented and discussed in Sec. III, and conclusions are summarized in Sec. IV.

II. EXPERIMENTAL

The experiment was performed at the Stanford Synchrotron Radiation Laboratory on a grazing-incidence "grasshopper" monochromator with a 1200 lines/mm holographically ruled grating. The ultrahigh-vacuum monochromator was vacuum isolated from our sample chamber by a 1500-Å-thick window. We used an aluminum window for energies below the aluminum $L_{2,3}$ edge at 72 eV, and we used a vitreous-carbon window for energies above 75 eV. For the spectra taken with second-order light about 280 eV, we again used the aluminum window.

The magnitude of the second-order light was determined by comparing the first- and second-order intensities of the neon $2p$ photoline. It was only appreciable ($>2\%$) at photon energies less than 150 eV with the carbon window. A correction for second-order light is necessary in the relative cross-section measurements, where the total light intensity, as monitored by a sodium salicylate scintillator and photomultiplier tube, is used to normalize the data at different photon energies. Because accurate measurements of the energy dependence of the sodium salicylate efficiency are not available, it was assumed to be constant.[11]

Photoelectron spectra were measured with the double-angle time-of-flight (DATOF) system, in which the pulsed time structure of the synchrotron radiation is used to measure the flight times of electrons ejected at two angles. This method has been described in detail elsewhere.[12,13]

The angular distribution of photoelectrons emitted by linearly polarized light in the nonrelativistic dipole approximation has the form

$$\frac{d\sigma(\epsilon,\theta)}{d\Omega}=\frac{\sigma(\epsilon)}{4\pi}[1+\beta(\epsilon)P_2(\cos\theta)] \ , \qquad (1)$$

where θ is the angle between the polarization vector of the radiation and the momentum vector of the photoelectron. By measuring electron spectra at two angles, it is possible to determine both the cross section $\sigma(\epsilon)$ and the angular distribution asymmetry parameter $\beta(\epsilon)$ as functions of electron energy ϵ. In this work, one analyzer was placed at $\theta=54.7°$, the "magic" angle where $P_2(\cos\theta)=0$, and another at $\theta=0°$. Cross-section measurements require knowing the relative transmission of the 54.7° analyzer as a function of kinetic energy and retarding voltage. The asymmetry-parameter measurements, however, only require knowing the ratio of the transmissions of the two analyzers. Calibration of the spectrometer is accomplished by measuring count rates for the neon $2s$ and $2p$ lines, for which $\sigma(\epsilon)$ and $\beta(\epsilon)$ are known.[14] We have corrected for the collection solid angle and an estimated linear polarization of 98%. However, because of the calibration procedures,[12] our derived $\beta(\epsilon)$ values are quite insensitive to the actual value of the polarization.

Representing the angular distribution by Eq. (1) assumes the validity of the dipole approximation, and it is important to know for what values of the photon energy, atomic number, and quantum numbers n and l this approximation is true. The measurements of cross sections at 54.7° (the "magic" angle) are also dependent upon Eq. (1). Kim *et al.*[15] found that for the inner shells of heavier elements multipole effects are important even at threshold. For outer subshells they found that the nondipole effects are small for photoelectron energies below 1 keV. Recent work by Wang *et al.*[16] has shown that while the quadrupole matrix element may be small, its contribution to low-energy angular distributions can be appreciable when the dipole intensity is at a minimum (e.g., a Cooper minimum). This would be particularly pronounced in s-subshell ionization where only $s\rightarrow\epsilon p$ matrix elements occur. For subshells with $l>0$, the $l\rightarrow\epsilon(l-1)$ dipole channel should still dominate over nondipole channels in regions where the $l\rightarrow\epsilon(l+1)$ dipole matrix element is small. We therefore expect the dipole approximation, and therefore Eq. (1), to be valid for all of the subshells addressed in this study.

The oven used to produce the mercury vapor was described earlier.[12] A vapor pressure of ~ 0.3 Torr (100 °C) was attained behind a 1.6-mm-diam nozzle. The temperature was monitored by a thermocouple, but the vapor-pressure corrections needed for cross-section measurements were determined by frequently repeating spectra.

Systematic errors introduced into the asymmetry parameter are probably less than 5% of the quantity $\beta+1$. For branching ratios, the probable magnitude of the errors will depend upon the difference between the kinetic energies of the two peaks. If the energy separation is large, the errors may be $\sim 5\%$; if small, the systematic error will be less. Additional random scatter in the absolute cross-section measurements, on the order of 10%, is due to uncertainty in the sample pressure correction. This scatter appears as correlated fluctuations in the cross sections of the different subshells and is not present in the branching ratios.

A representative spectrum is shown in Fig. 1. The observed photoelectron lines are listed in Table I, along with their binding energies (BE). In addition to the lines in Table I, a set of $N_{6,7}O_{4,5}O_{4,5}$ Auger lines with constant kinetic energies between 59 and 72 eV were observed.[17]

A retarding cage inside each analyzer allows us to slow the electrons for the final 17 cm of the 28-cm path length. The analyzer resolution, which results

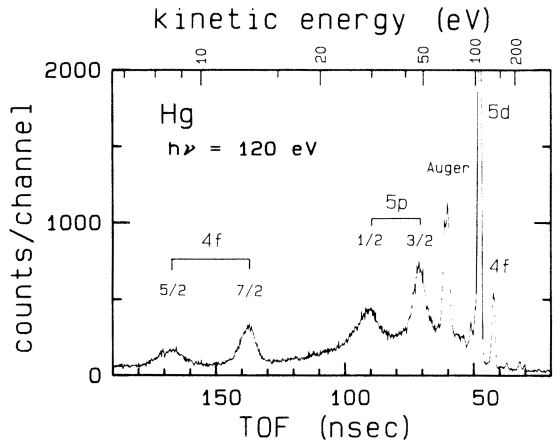

FIG. 1. TOF photoelectron spectrum of Hg taken at $\theta=54.7°$. There are 5.08 channels/nsec, and the accumulation time was 500 sec. $4f$ peak at 131 eV is due to second-order light with $h\nu=240$ eV. $5d$ peak reaches a maximum of 5200 counts/channel.

primarily from the finite interaction volume, was $\sim 3\%$ of the kinetic energy after retarding. Retarding potentials up to 115 V were used to resolve the $4f$ and $5d$ spin-orbit doublets. Generally, the analyzer and monochromator resolutions were adjusted to provide a total resolution [full width at half maximum (FWHM)] of <2 eV for the $4f$ doublet and, for some spectra, <1 eV for the $5d$ doublet. We deconvoluted some of these doublets by a least-squares fitting method that used Gaussian functions with low-energy exponential tails. The weak $5p_{1/2}$ and $5p_{3/2}$ peaks have large natural linewidths (6.2 and 5.6 eV, respectively).[3] The $5p$ peaks were fitted by Lorentzians with fixed widths and, where possible, fixed doublet spacings.

The error bars for the fitted data represent standard deviations from the computer fits. For the raw data the error bars represent counting statistics only.

TABLE I. Binding energies in electron volts for observed mercury subshells.

Subshell	Binding energy (from Ref. 4)
$5d_{5/2}$	14.9
$5d_{3/2}$	16.7
$5p_{3/2}$	71.6
$5p_{1/2}$	90.3
$4f_{7/2}$	107.1
$4f_{5/2}$	111.1

III. RESULTS AND DISCUSSION

The format of this section will be to describe in each subsection a derived parameter (e.g., cross section) for all three subshells, with a discussion given in text for each subshell. A summary paragraph appears at the end of each subsection.

A. Cross sections

To put our cross-section data on an absolute scale it is necessary to have an experimental measurement of the total cross section at one energy. Using the absorption data of Cairns *et al.*,[18] with the adjustment of Dehmer and Berkowitz,[19] we have normalized our data so that the $5d$ partial cross section is 8 Mb at 70 eV. We note that the adjustment in Ref. 19 is only approximate, but should be good to within 30%. We have plotted all of the theoretical curves, which were given in terms of kinetic energy, from the experimental thresholds, thus eliminating energy shifts due to the different choices of thresholds in the calculations.

In Fig. 2 our $5d$ cross-section measurements are plotted, together with earlier absorption measurements and the RRPA and DS curves. Two RRPA curves are represented in Fig. 2. The calculated curve[20] below 65 eV included interchannel coupling with the $6s$ channels, while for higher energies, the calculation[10] included coupling with the $4f$ and $5p$ channels. These different sets of coupled channels are probably responsible for the discontinuity between the two curves at 65 eV. Both data and theories show the 100-fold decrease from 50 eV to

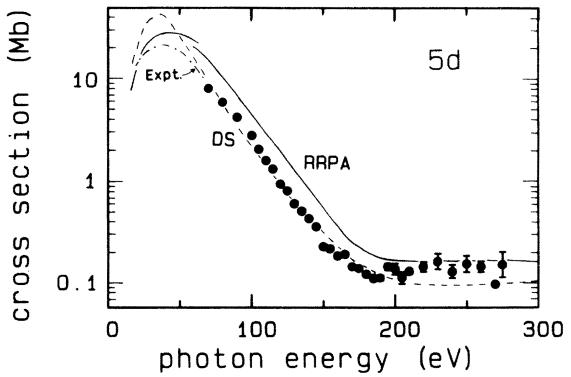

FIG. 2. $5d$ cross section. Solid curves represent the RRPA calculations (Refs. 10 and 20). There is a discontinuity between the two calculations near 65 eV. Dashed curve represents the DS calculation (Ref. 8). Dashed-dotted curve is from absorption measurements (Refs. 18 and 19). Data were normalized to σ (70 eV) = 8 Mb. This sets the scale for all our cross-section data.

the Cooper minimum, which can be seen near 190 eV in the data. The minimum is not apparent in the theoretical curves. Above 190 eV, the DS curve lies significantly below the data. Above 70 eV, the RRPA curve has about the same shape as the DS curve, but its magnitude is larger by a factor of 2. Neither of the calculations include core relaxation or double ionization. A Dirac-Fock calculation that includes core relaxation has been performed[21] below 55 eV, and it gives better agreement than either the DS or RRPA calculations.

Although the 6*s* photoelectron peak (BE=10.4 eV) is unresolved from the 5*d* peak in almost all of our spectra, we expect its effect to be insignificant, because the cross section for the 6*s* subshell is much smaller than that for the 5*d* subshell above 70-eV photon energy.

The 4*f* cross section is plotted in Fig. 3. The large centrifugal barrier acting on the ϵg continuum electrons causes a "delayed onset" of the 4*f* cross section, clearly exhibited in the data. In fact, the decrease in the $4f \rightarrow \epsilon d$ partial cross section can be seen below 150 eV, before the ϵg contribution to the 4*f* cross section becomes dominant. Both the RRPA and the DS curves show larger fractional increases than the data between 150 and 270 eV, but the RRPA curve agrees better with the data both in this respect and in the position of the minimum. The RRPA 4*f*:5*d* branching ratio (not shown) is in good agreement with our measurements below 170 eV, while it deviates by a factor of 2 near 270 eV.

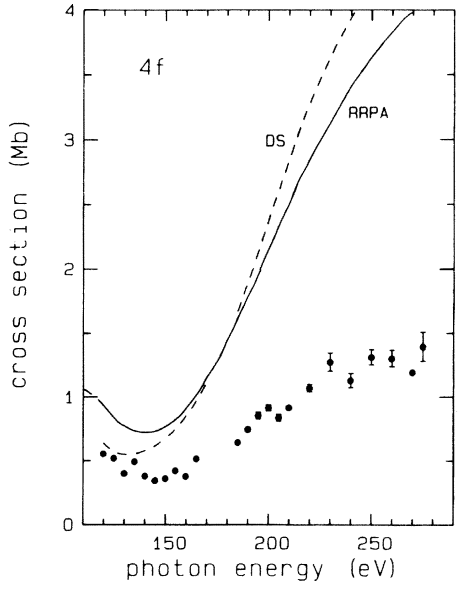

FIG. 3. 4*f* cross section. Solid curve, RRPA length from Ref. 10; dashed curve, DS from Ref. 8.

The agreement of this ratio with the DS theory is significantly worse.

The $5p_{3/2}$ and $5p_{1/2}$ cross sections are plotted in Fig. 4. In both subshells, the experimental cross section below 180 eV drops more quickly than the theoretical curves. The changes in curvature in $\sigma(5p_{3/2})$ near 180 eV and in $\sigma(5p_{1/2})$ near 190 eV are assigned to Cooper minima in these subshells.

In summary, the experimental cross sections generally show the expected energy variations, with minima being readily observed in every case. The 4*f* delayed onset character due to the angular momentum barrier for the *g* wave is clearly present. The RRPA cross sections are a factor of 2 too large. However, the RRPA calculated 4*f*:5*p*:5*d* branching ratios generally agree to within 10%, with the notable exceptions being those involving $\sigma(4f)$ above 200 eV and $\sigma(5p)$ below 160 eV. The DS calculated 5*p* and 5*d* cross sections are in better agreement with experiment.

B. Spin-orbit branching ratios

Deviations of spin-orbit branching ratios from their statistical $(l+1)/l$ value arise from the "kinetic-energy" effect,[22] caused by the photoelectrons from the two spin-orbit members having different kinetic energies at a given photon energy. Additional deviations are due to differences in the

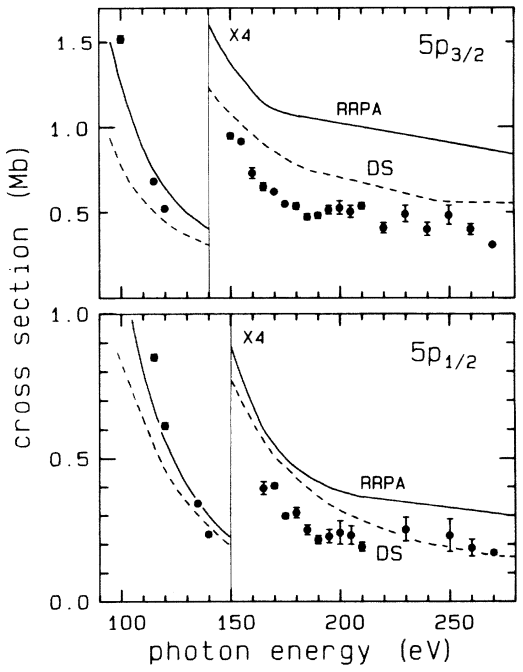

FIG. 4. Cross section of the $5p_{3/2}$ (upper) and $5p_{1/2}$ (lower) states. RRPA curves are from Ref. 10 and the DS curves are from Ref. 8.

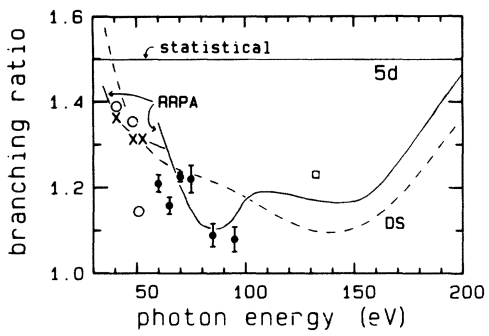

FIG. 5. $5d_{5/2}$:$5d_{3/2}$ subshell branching ratio. Solid circles are from this work; open circles from Ref. 24; ×'s from Ref. 25; square from Ref. 4. Two lower energy ×'s coincide with measurements from Ref. 19. Solid curves are from two RRPA calculations (Refs. 10 and 20); dashed curve, DS theory (Ref. 8). Accuracy of the first two open-circled measurements are ±20% and the third ±40%. No estimates of the uncertainties for the other line-source measurements were published.

radial wave functions of the initial and final states. Ron, Kim, and Pratt[23] have recently surveyed some of the non—kinetic-energy effects that cause deviations in subshell branching ratios. They found that, for higher-Z elements, deviations are amplified by the presence (and by the energy separation) of Cooper minima in dominant channels. They also concluded that these effects should be larger for np subshells than for nd or nf subshells.

The DS (Ref. 8) and RRPA (Refs. 10 and 20) calculations of the $5d_{5/2}$:$5d_{3/2}$ branching ratio are shown in Fig. 5, along with experimental points from this work and from experiments with line sources. The $5d$ cross section (Fig. 2) has a large shape resonance peaking near 40-eV photon energy and a Cooper minimum near 190 eV. The experimental branching ratio starts well above the statistical value near threshold[2] and then drops monotonically to a minimum value of ~1.1 near 90 eV. The DS theory predicts this trend qualitatively, while the RRPA result shows an additional feature at 85 eV that may be due to intershell correlations with the $5p$ subshell. The RRPA curves above and below 65 eV do not join smoothly, presumably due to the different sets of coupled channels used in the two calculations, as mentioned earlier in connection with the $5d$ cross section. This point needs further study.

The $4f$ subshell cross section has no Cooper minimum because the $4f$ radial wave function has no nodes, but there is a shape resonance due to the ϵg centrifugal barrier, and a cross-section minimum near 150 eV. Our $4f$ branching-ratio data are shown in Fig. 6 with a curve predicted by both the RRPA and DS theories. The curve shows a maximum in the branching ratio between 150 and 200 eV. Our branching-ratio measurements confirm the existence of a maximum rising above 1.5, but the detailed shape is unclear from the data because of nonstatistical scatter arising from uncertainties in background corrections. The slower increase in the measured cross section than in the calculated cross sections above 160 eV (Fig. 3) should appear as a smaller branching ratio, due to the kinetic-energy effect. This is apparent near 200 eV in Fig. 6.

The large spin-orbit splitting in the $5p$ subshell (18.6 eV) leads to large deviations in the branching ratio from its statistical value of 2.0. Calculations of the $5p \rightarrow \epsilon s$ and $5p \rightarrow \epsilon d$ cross sections by Keller and Combet Farnoux[6] show that the ϵs channel is dominant for the first 200 eV above threshold and that the ϵd channel goes through a Cooper minimum. The RRPA calculation[10] of the branching ratio shown in Fig. 7 shows an increase from ~1.1 at 110 eV to ~2.8 at 220 eV. Our data show

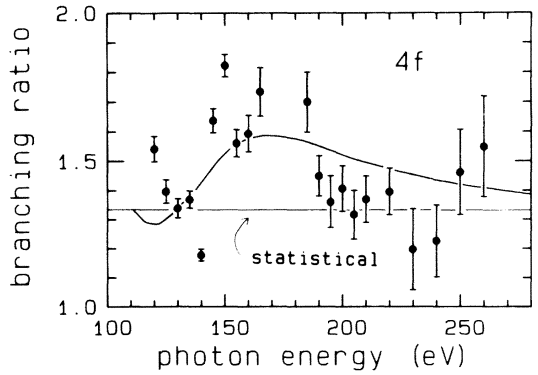

FIG. 6. $4f_{7/2}$:$4f_{5/2}$ branching ratio. Solid curve from RRPA (Ref. 10). DS theory (Ref. 8), also follows the solid curve.

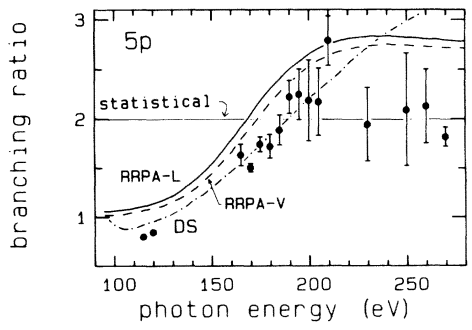

FIG. 7. $5p_{3/2}$:$5p_{1/2}$ branching ratio. Solid curve (RRPA, length) and dashed curve (RRPA, velocity) are taken from Ref. 10. DS curve is taken from Ref. 8.

the ratio starting near 0.85 at 25 eV above the $5p_{1/2}$ threshold and increasing to ~ 2.2 at $h\nu = 200$ eV. The DS curve is in much better agreement with the data. The gap in the data arises from the Auger group moving through the $5p$ lines. A much more careful study would be required to fill in the gap.

In summary, deviations from statistical ratios, and variations with energy, were observed for all three subshells. Both RRPA and DS theory predicted the experimental ratios quite well, although the RRPA is in better agreement for the $5d$ subshell, and the DS is in better agreement for the $5p$ subshell. Evidence was found for a large kinetic-energy effect in the $5p$ subshell and for a small shape resonance effect in the $4f$ subshell. The RRPA theory alone predicted details in the $5d$ curve that may arise from interchannel coupling. More experimental work is clearly needed on these branching ratios.

C. Asymmetry parameters

The energy variation of the calculated angular distribution asymmetry parameter $\beta(\epsilon)$ often complements the variations in the cross section and branching ratio. In the case of Cooper minima, the predicted effects on the $\beta(\epsilon)$ parameter are typically more pronounced than the effects on the other parameters. Few data are available to test these predictions. For example, we report below the *first* $\beta(\epsilon)$ measurements on any $4f$ and $5d$ subshells over a substantial energy range.

The $5d$-subshell $\beta(\epsilon)$ parameter shows large oscillations. These are due to a Coulomb phase-shift change just above threshold,[15] then a shape resonance, and then a Cooper minimum. Using the central-field approximation, the $\beta(\epsilon)$ parameter is given in LS coupling by the Cooper-Zare formula[26]

$$\beta(\epsilon)=\frac{(l-1)R_{l-1}^2+(l+1)(l+2)R_{l+1}^2-6l(l+1)R_{l-1}R_{l+1}\cos(\Delta_{l+1,l-1})}{(2l+1)[lR_{l-1}^2+(l+1)R_{l+1}^2]} , \tag{2}$$

where R_{l+1} and R_{l-1} are radial dipole matrix elements and $\Delta_{l+1,l-1}$ is their phase difference. At a Cooper minimum, where $R_{l+1}=0$, Eq. (2) simplifies to

$$\beta(R_{l+1}=0)=\frac{l-1}{l(2l+1)} . \tag{3}$$

Equations (2) and (3) were derived neglecting configuration interaction, fine-structure splitting, and the spin-orbit interaction between the outgoing electron and the ion. If we ignore these complications, we find that the Cooper minimum for the $5d$ subshell should be located where $\beta(\epsilon)$ reaches 0.1, which is at 190 eV in Fig. 8. The data in Fig. 2 confirm this value, whereas the theoretical curves do not show a minimum.

The DS and RRPA curves for $\beta(\epsilon)$ are generally in good agreement with our data, but they differ by 10–20 eV in the energy of greatest negative slope and in the value of $\beta(\epsilon)$ for energies above the Cooper minimum. It may be that the position of the Cooper minimum, which is due to a cancellation in the R_f radial integral, is extremely sensitive to both the accuracy of the integrating code and the nature of the theory. A similar sensitivity was observed in the position and depth of the minimum in $\beta(\epsilon)$ for the Xe $5s$ Cooper minimum.[29]

The theoretical curves of $\beta(\epsilon)$ for the unresolved $4f$ subshell, together with our results, are displayed in Fig. 9. All of these theories show the same gen-

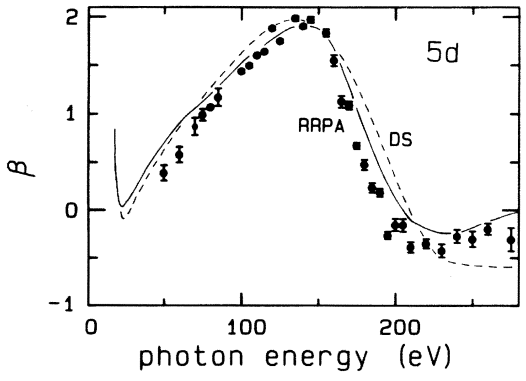

FIG. 8. $5d$ angular distribution asymmetry parameter. Solid curve is RRPA (Refs. 10 and 20); dashed curve, DS from Ref. 8. Experimental measurements below 45 eV (Refs. 27 and 28) are in excellent agreement with the RRPA curve.

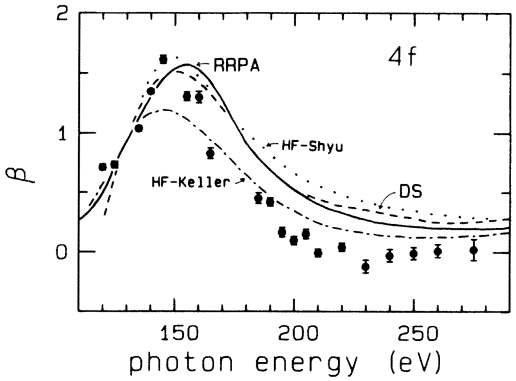

FIG. 9. $4f$ asymmetry parameter. Theoretical curves are solid, RRPA (Ref. 10); dashed-dotted, HF (Ref. 6); dotted, HF (Ref. 5); dashed, DS theory (Ref. 8).

eral features, but none reproduce the data quantitatively. The most sophisticated of the theories (RRPA) has the energy of the maximum in $\beta(\epsilon)$ 10 eV too high and the $\beta(\epsilon)$ curve above 200 eV 0.2β units too large.

The two $4f$ spin-orbit members have different $\beta(\epsilon)$ values at a given photon energy. Most of this difference results from a kinetic-energy effect. In Fig. 10, we have plotted $\beta(\frac{7}{2})$-$\beta(\frac{5}{2})$ against photon energy along with the RRPA calculated curve. The differences calculated from DS theory are almost identical. The data and the theory are in qualitative agreement.

Figure 11 shows $\beta(\epsilon)$ for the $4f$ subshell from threshold to a photon energy of 600 eV. All but three of the points above 280 eV were taken using second-order light and an aluminum window. The calibration of the relative efficiencies of the analyzers was done with second-order Ne $2s$ and $2p$ photoelectrons. The uncertainty in the calibration for kinetic energies above 300 eV introduces an uncertainty in the slope of the data in Fig. 11 ($\sim 0.2\beta$ units at $h\nu = 600$ eV). The calibration is, however, a smooth function. The sudden increase in $\beta(\epsilon)$ at 380 eV is probably the result of interchannel coupling with the $4d$ ionization channels. Using first-order perturbation theory, each $4f$ transition amplitude is the sum of a direct and a correlation amplitude, the latter resulting from a virtual excitation of the $4d$ subshell.[30] This correlation amplitude can affect both the $4f$ cross section and the $4f$ angular distribution.

The $4d_{5/2}$ and $4d_{3/2}$ thresholds are at 366.0 and 385.4 eV, respectively,[3] where the monochromator bandpass was approximately 7 eV. The DS calculations of the $4d$ subshell[9] show its cross section to be a factor of 10 less than the $4f$ cross section at 400 eV. The calculated $4d$ spin-orbit branching ratio[31] and the $\beta(\epsilon)$ parameter[9,31] are calculated to have large fluctuations near threshold which may be manifesting themselves in the $4f$ $\beta(\epsilon)$. We were unable to measure the $4d$ photoelectron peaks directly because of their small cross sections and large natural linewidths (4 eV).

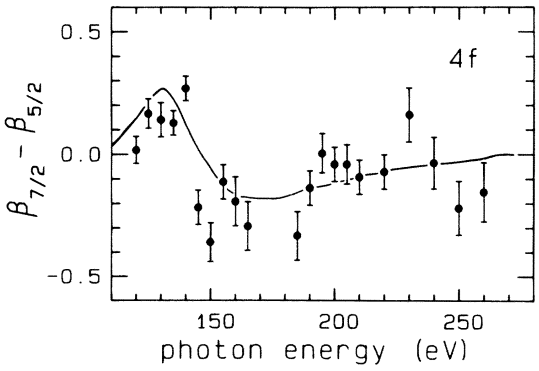

FIG. 10. Difference between the $4f_{7/2}$ and $4f_{5/2}$ $\beta(\epsilon)$ parameters. Solid curve is the RRPA calculation from Ref. 10 which is almost identical to the DS curve from Ref. 8.

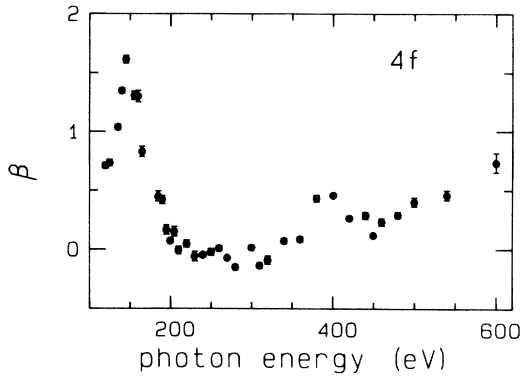

FIG. 11. $4f$ asymmetry parameter.

Large changes in $\beta(\epsilon)$ due to coupling with newly opened channels have been observed in $\beta_{5p}(\epsilon)$ at the $4d$ threshold in Xe.[32] However, in the Xe case the $4d$ cross section near threshold is much larger than the cross section of the $5p$ subshell.

Figure 12 shows the $5p_{1/2}$ and $5p_{3/2}$ asymmetry-parameter measurements. Again, the gaps in these data are caused by the presence of Auger electrons.

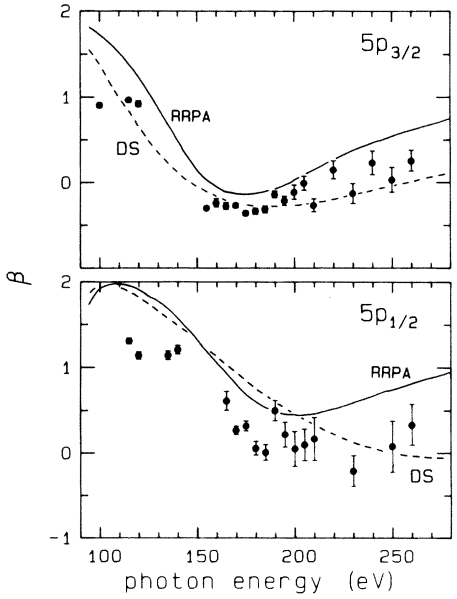

FIG. 12. Asymmetry parameter $\beta(\epsilon)$ for the $5p_{3/2}$ (top panel) and $5p_{1/2}$ (lower panel) states. RRPA curves are from Ref. 10 and the DS curves are from Ref. 8.

The two states show substantial differences beyond that due to the kinetic-energy effect. Our data show $\beta(5p_{1/2})$ dropping to zero, while $\beta(5p_{3/2})$ drops to a value of -0.3. The minimum in each parameter is due to a Cooper minimum in the ϵd channels. If we apply Eq. (3), we would expect the unresolved $\beta_{5p}(\epsilon)$ to drop to zero. Because we have measured the resolved $\beta(\epsilon)$'s it may be more appropriate to know what value of $\beta(\epsilon)$ we would expect at the minimum in the limit of jj coupling. Walker and Waber[22] have shown that for s-subshell ionization ($j=\frac{1}{2}$), in which only two relativistic continuum channels are accessible, the expression for $\beta(\epsilon)$ takes on a simple form in jj coupling:

$$\beta(\epsilon,j=\tfrac{1}{2})=\frac{2R_{3/2}^2+4\,|\,R_{3/2}R_{1/2}^*\,|}{R_{1/2}^2+2R_{3/2}^2} \quad . \tag{4}$$

For ionization from a $p_{1/2}$ subshell (again $j=\frac{1}{2}$), the expression for $\beta(\epsilon)$ is identical. For the $p_{1/2}$ subshell, $R_{1/2}$ and $R_{3/2}$ are radial matrix elements with the $\epsilon s_{1/2}$ and $\epsilon d_{3/2}$ continuum orbitals. When the $R_{3/2}$ matrix element equals zero we obtain $\beta(5p_{1/2})=0$, in agreement with experiment. It is not as easy to apply Walker and Waber's formalism to $\beta(5p_{3/2})$ because there are three continuum orbitals ($\epsilon s_{1/2}$, $\epsilon d_{3/2}$, and $\epsilon d_{5/2}$) and the $R_{3/2}$ and $R_{5/2}$ matrix elements (for the ϵd channels) need not go through zero at the same energy. If they did we would again obtain $\beta=0$. Of course, in the general many-electron case the radial matrix elements are complex and need not go identically to zero.

The RRPA calculation of $\beta(5p_{1/2})$ shows $\beta(\epsilon)$ falling only to 0.5. This is a result of mixing with the $4f$-subshell ionization channels, because an 11-channel calculation, which includes only the $5p$ and $5d$ subshells, shows $\beta(5p_{1/2})$ dropping to 0.0 at 280 eV.[31] The DS calculation is significantly closer to experiment for the $5p_{3/2}$ subshell, but not for the $5p_{1/2}$ subshell.

In summary, the asymmetry parameter of the mercury $4f$, $5p$, and $5d$ subshells behave approximately as predicted by the DS and RRPA models, but there are important differences between experiment and theory. Both theories predict the centrifugal-barrier induced maxima in the $4f$ subshell to be too wide, with the consequent overestimation of the photon energies where $\beta(\epsilon)$ decreases most rapidly. In addition, a feature was observed in $\beta(4f)$ at 380 eV which we attribute to interaction with the $4d$-ionization channels.

IV. CONCLUSIONS

Several noteworthy features have been exhibited in the photoionization of Hg above 50 eV. The Cooper minimum in the $5d$-subshell photoionization is observed in both the cross section and the asymmetry parameter. The $5d$ branching ratio was found to drop as low as 1.1, although we were unable to test the RRPA prediction that shows oscillating features due to interaction with $5p$-subshell ionization.

In the $4f$ subshell, the centrifugal barrier in the ϵg channel was observed as a shape resonance in the asymmetry parameter and as a delayed onset in the cross section. An additional oscillation in $\beta(\epsilon)$ has been attributed to interaction with $4d$-subshell ionization.

The $5p$ subshell, which has the largest spin-orbit splitting, was found to have a branching ratio of 0.85 at low kinetic energies. The two spin-orbit members were found to have different values of β at their respective Cooper minima.

The DS and RRPA theories correctly predict the shapes of all of the parameters, although there are several quantitative differences. Among these, the delayed onset of the $4f$ cross section shows the worst agreement. There is good agreement with the $5f$:$5p$:$5d$ branching ratios calculated by RRPA, but there is a factor of 2 difference between the calculated absolute cross sections and the present results. The DS cross sections are in better agreement with experiment. Experimentally, there is a need for a reliable absolute absorption measurement, as well as measurements of the Hg^{2+}/Hg^{+} ratio.

ACKNOWLEDGMENTS

The authors thank V. Radojević and S. T. Manson for helpful discussions and for providing their calculations prior to publication. This work was supported by the Director, Office of Energy Research, Office of Basic Energy Sciences, Chemical Sciences Division of the U. S. Department of Energy under Contract No. DE-AC03-76SF00098. It was performed at the Stanford Synchrotron Radiation Laboratory, which is supported by the National Science Foundation through the Division of Materials Research. One of us (H.G.K.) would like to acknowledge support by a Wigner fellowship.

*Permanent address: Fachbereich Physik, Technische Universität Berlin, D-1000 Berlin 12, West Germany.

[1]J. P. Connerade and M. W. D. Mansfield, Proc. R. Soc. London, Ser. A 335, 87 (1973).

[2]S. P. Shannon and K. Codling, J. Phys. B 11, 1193 (1978) and references therein.

[3]R. Nilsson, R. Nyholm, A. Berndtsson, J. Hedman, and C. Nordling, J. Electron Spectrosc. 9, 337 (1976).

[4]S. Svensson, N. Martensson, E. Basilier, P. Å. Malmqvist, U. Gelius, and K. Siegbahn, J. Electron Spectrosc. 9, 51 (1976).

[5]J. S. Shyu and S. T. Manson, Phys. Rev. A 11, 166 (1975).

[6]F. Keller and F. Combet Farnoux, J. Phys. B 12, 2821 (1979).

[7]T. E. H. Walker and J. T. Waber, J. Phys. B 7, 674 (1974).

[8]B. R. Tambe and S. T. Manson (private communication).

[9]F. Keller and F. Combet Farnoux, J. Phys. B 15, 2657 (1982).

[10]V. Radojević and W. R. Johnson, Phys. Lett. 92A, 75 (1982).

[11]J. A. R. Samson and G. N. Haddad, J. Opt. Soc. Am. 64, 1346 (1974).

[12]S. Southworth, C. M. Truesdale, P. H. Kobrin, D. W. Lindle, W. D. Brewer, and D. A. Shirley, J. Chem. Phys. 76, 143 (1982).

[13]P. H. Kobrin, U. Becker, S. Southworth, C. M. Truesdale, D. W. Lindle, and D. A. Shirley, Phys. Rev. A 26, 842 (1982).

[14]F. Wuilleumier and M. O. Krause, J. Electron Spectrosc. 15, 15 (1979).

[15]Y. S. Kim, R. H. Pratt, A. Ron, and H. K. Tseng, Phys. Rev. A 22, 857 (1980).

[16]M. S. Wang, Y. S. Kim, R. H. Pratt, and A. Ron, Phys. Rev. A 25, 857 (1982).

[17]H. Aksela, S. Aksela, J. S. Jen, and T. D. Thomas, Phys. Rev. A 15, 985 (1977).

[18]R. B. Cairns, H. Harrison, and R. I. Schoen, J. Chem. Phys. 53, 96 (1970).

[19]J. L. Dehmer and J. Berkowitz, Phys. Rev. A 10, 484 (1974).

[20]W. R. Johnson, V. Radojević, P. Deshmukh, and K. T. Cheng, Phys. Rev. A 25, 337 (1982).

[21]B. R. Tambe, W. Ong, and S. T. Manson, Phys. Rev. A 23, 799 (1981).

[22]T. E. H. Walker and J. T. Waber, J. Phys. B 6, 1165 (1973).

[23]A. Ron, Y. S. Kim, and R. H. Pratt, Phys. Rev. A 24, 1260 (1981).

[24]S. Süzer, P. R. Hilton, N. S. Hush, and S. Nordholm, J. Electron Spectrosc. 12, 357 (1977).

[25]S. Süzer, S. T. Lee, and D. A. Shirley, Phys. Rev. A 13, 1842 (1976).

[26]J. Cooper and R. N. Zare, *Lectures in Theoretical Physics: Atomic Collision Processes,* edited by S. Geltman, K. T. Mahanthappa, and W. E. Brittin (Gordon and Breach, New York, 1969), Vol. XIC, pp. 317–337.

[27]G. Schönhense, J. Phys. B 14, L187 (1981).

[28]A. Niehaus and M. W. Ruff, Z. Phys. 252, 84 (1972).

[29]M. G. White, S. H. Southworth, P. Kobrin, E. D. Poliakoff, R. A. Rosenberg, and D. A. Shirley, Phys. Rev. Lett. 43, 1661 (1979).

[30]M. Ya Amusia and V. K. Ivanov, Phys. Lett. 59A, 194 (1976).

[31]V. Radojević and W. R. Johnson (private communication).

[32]M. O. Krause, T. A. Carlson, and P. R. Woodruff, Phys. Rev. A 24, 1374 (1981).